JOURNAL OF MAGNETIC RESONANCE **129,** 85–92 (1997)
ARTICLE NO. MN971242

Coupling Amplification in 2D MAS NMR and Its Application to Torsion Angle Determination in Peptides

Mei Hong,* John D. Gross,* Chad M. Rienstra,* Robert G. Griffin,*[,1]
Kristin K. Kumashiro,†[,2] and Klaus Schmidt-Rohr†

*Francis Bitter Magnet Laboratory and Department of Chemistry, Massachusetts Institute of Technology, Cambridge, Massachusetts 02139; and †Department of Polymer Science and Engineering, University of Massachusetts, Amherst, Massachusetts 01003

Received May 28, 1997

A technique for amplifying the apparent magnitudes of $^{13}C-^{1}H$ and $^{15}N-^{1}H$ dipolar interactions in magic-angle spinning experiments is described. By inserting rotor-synchronized 180° pulses in the evolution period of a 2D dipolar-chemical shift experiment, heteronuclear dipolar couplings are doubled or quadrupled relative to the spinning speed. The increased number of dipolar sidebands is desirable for retaining structural information in the indirectly detected dipolar dimension while resolving inequivalent sites in the isotropic chemical shift dimension at relatively high spinning speeds. This coupling amplification method is incorporated into an experiment that determines the peptide torsion angle ϕ through the relative orientation of the $C^{\alpha}-H^{\alpha}$ and $N-H^{N}$ bonds. It is shown both experimentally and theoretically that the angular resolution of the measurement is enhanced significantly by the selective doubling of the $N-H^{N}$ coupling. © 1997 Academic Press

Key Words: **solid-state NMR; dipolar coupling; magic-angle spinning; torsion angle; peptide structure.**

INTRODUCTION

Heteronuclear dipolar interactions have long been recognized as useful probes of bond lengths and orientations in solids. For example, $^{13}C-^{1}H$ and $^{15}N-^{1}H$ couplings detected under homonuclear proton decoupling were used for determining internuclear distances, for relating chemical shift tensors to bond directions, and for observing fast molecular motions (*1–6*). Recently, they have found new uses in NMR experiments that permit measurement of torsion angles through the relative orientation of molecular segments (*7–9*). Many of these experiments employ magic-angle spinning (MAS) to provide site resolution and spectral sensitivity. However, since MAS confines the spectral intensity to rotational sidebands, the information content of the spectra is optimized in the slow spinning regime. At spinning speeds $\omega_r/2\pi > \delta_d/3$, where δ_d is the dipolar coupling strength, the dipolar spectrum is dominated by an uninformative centerband. For a one-bond N–H dipolar coupling measured with MREV-8 homonuclear decoupling, $\delta_d \approx 4.5$ kHz and the centerband dominates for spinning speeds as low as $\omega_r/2\pi \approx 1.5$ kHz. While low spinning speeds are desirable for extracting structural information, the necessity of resolving different chemical moieties through isotropic chemical shifts results in an opposing constraint. Higher spinning speeds average the chemical shift anisotropy (δ_{CSA}) more completely and thus yield better-resolved spectra. This conflict is exacerbated at higher magnetic field strengths, since shift anisotropies scale linearly with the field strength while the dipolar couplings are field-independent. Thus, the desirable spinning speed range $\delta_{CSA} \ll \omega_r \ll \delta_d$ is reduced at the higher magnetic fields, making it more difficult to observe dipolar sideband spectra and sideband-free isotropic shift spectra simultaneously. Methods for suppressing chemical shift sidebands such as TOSS and SELTICS (*10–12*) have the disadvantage of inducing signal losses in the direct dimension at slow MAS rates. In addition to the chemical shift anisotropy, the homonuclear dipolar interaction among the low-γ spins has also become a source of line broadening in the chemical shift spectrum, as uniformly or fractionally labeled molecules are increasingly used for the study of biomolecular structures. Again, the most convenient way of minimizing this broadening is to employ higher spinning speeds.

In order to obtain informative dipolar sideband patterns in the ω_1 dimension and simple spectra in ω_2 of a 2D dipolar-chemical shift (DIPSHIFT) spectrum without changing the spinning speed, it is desirable to amplify the apparent dipolar coupling strengths in ω_1 by rotor-synchronized 180° pulses. These 180° pulses are employed such that they define the evolution period of a DIPSHIFT experiment in which a MREV-8 multiple-pulse train is applied for a fixed number of rotor periods. As a result, the dipolar couplings of interest are amplified with respect to the spinning speed. The technique is based on a sequence first employed in REDOR experiments (*13*), and is closely re-

[1] To whom correspondence should be addressed at NW14-3220, Francis Bitter Magnet Laboratory, Massachusetts Institute of Technology, Cambridge, MA 02139-4307. Fax: (617) 253-5405. E-mail: griffin@ccnmr.mit.edu.

[2] Current address: Department of Chemistry, University of Hawaii at Manoa, 2545 The Mall, Honolulu, HI 96822.

1090-7807/97 $25.00

lated to earlier MAS experiments that achieve sideband enhancement (*14–16*).

As a practical example of the amplification of the X–^{1}H (e.g., X = ^{13}C, ^{15}N) dipolar interaction under MAS, we show the result of increasing the number of dipolar sidebands in a recently introduced experiment (*8*) that correlates the relative orientation of the N–H^{N} and C$^{\alpha}$–H$^{\alpha}$ bonds in order to determine the peptide torsion angle ϕ. The relative orientation is observed in the sum and difference frequencies of the N–H and C–H dipolar couplings, which are measured under homonuclear decoupling of the protons. However, there were two restrictions in this NH/C$^{\alpha}$H experiment. First, it required low spinning speeds of about 2.5 kHz in order to generate a sufficient number of sidebands in the dipolar dimension. Second, the ϕ dependence of the spectra is small in certain angular regions, thus limiting the ability to distinguish similar secondary structures such as the right-handed α helix and the 3_{10} helix. We now show that not only can the spinning speed constraint be relaxed, but the spectral variation with ϕ can also be enhanced by doubling the effective N–H coupling while keeping the C–H coupling unchanged. In other words, both the spectral and the angular resolutions of the NH/C$^{\alpha}$H technique can be improved by coupling amplification.

THEORY

1. Interaction ''Doubling'' under MAS

In a MAS rotor period unperturbed by RF pulses, the dynamic phase Φ acquired by a spin due to the interaction λ after time t_1 is

$$\begin{aligned}\Phi(t_1) &= \int_0^{t_1} \omega(t)dt \\ &= \delta_\lambda \int_0^{t_1} dt(g_1\cos(\omega_r t + \psi_1) \\ &\qquad + g_2\cos(2\omega_r t + \psi_2)),\end{aligned} \qquad [1]$$

where the coefficients g_1 and g_2 and the phase angles ψ_1 and ψ_2 are functions of the Euler angles (α, β, γ) that describe the orientation of the principal axis system in a rotor-fixed coordinate system and of the asymmetry η of the interaction (*17, 18*), and δ_λ is the anisotropy of the interaction. After each full rotation period during which the spin interaction is active, the phase averages to zero

$$\Phi(\tau_r) = \int_0^{\tau_r} \omega(t)dt = 0, \qquad [2]$$

indicating refocusing of the interaction. A 180° pulse applied at time t_1 in the rotor period inverts the phase of the magnetization so that the overall phase at the end of the rotor cycle becomes

$$\begin{aligned}\Phi(\tau_r) &= -\int_0^{t_1} \omega(t)dt + \int_{t_1}^{\tau_r} \omega(t)dt \\ &= -\int_0^{t_1} \omega(t)dt + \left(\int_0^{\tau_r} \omega(t)dt - \int_0^{t_1} \omega(t)dt\right) \\ &= -2\int_0^{t_1} \omega(t)dt + \int_0^{\tau_r} \omega(t)dt \\ &= -2\int_0^{t_1} \omega(t)dt = -2\Phi(t_1).\end{aligned} \qquad [3]$$

The phase in Eq. [3] is twice that of the evolution in Eq. [1]. Since $\Phi(t)$ is proportional to δ_λ, this doubling of the dynamic phase can be viewed as an effective doubling of the anisotropy δ_λ at the spinning speed ω_r. Alternatively, since

$$2\Phi(t_1, \omega_r) = \Phi(2t_1, \omega_r/2), \qquad [4]$$

the doubling of the phase is also equivalent to an effective reduction of the spinning speed ω_r by half while the coupling strength δ_λ remains constant.

The simple pulse sequence described above is applicable to NMR interactions that are linear in the spin to which the 180° pulse is applied. Thus, the anisotropic chemical shift and the heteronuclear dipolar couplings are suitable interactions to be manipulated. For X–^{1}H dipolar couplings, two versions of the experiment are possible. Both involve a constant-time evolution period of two rotor cycles, where on the ^{1}H channel homonuclear multiple-pulse decoupling is applied during the first rotor cycle and heteronuclear dipolar decoupling is applied during the second. In the first experimental version (Fig. 1a), two 180° pulses are applied on the X spins at t_1 and $\tau_r + t_1$. The X–^{1}H dipolar evolution is doubled by the first 180° pulse and unaffected by the second, while the X-spin chemical shift is refocused by both 180° pulses upon completion of the two rotor periods. In the second version of the experiment (Fig. 1b), a proton 180° pulse is applied at t_1, while an X-spin 180° pulse is applied at τ_r to refocus the isotropic chemical shift. The X anisotropic chemical shift is removed by magic-angle spinning. Both versions of the experiment yield 2D DIPSHIFT spectra in which the dipolar dimension exhibits effectively doubled coupling strength.

The effects of the 180° pulses on the formation of the dipolar spin echoes in MAS experiments have been examined in detail previously (*16, 19–21*). There, 180° pulses were similarly employed on the protons or the rare spins to perturb the formation of rotational echoes, leading to enhanced chemical shift or dipolar sidebands. However, there are two important differences between these previous experiments and the current version. In the previous experiments,

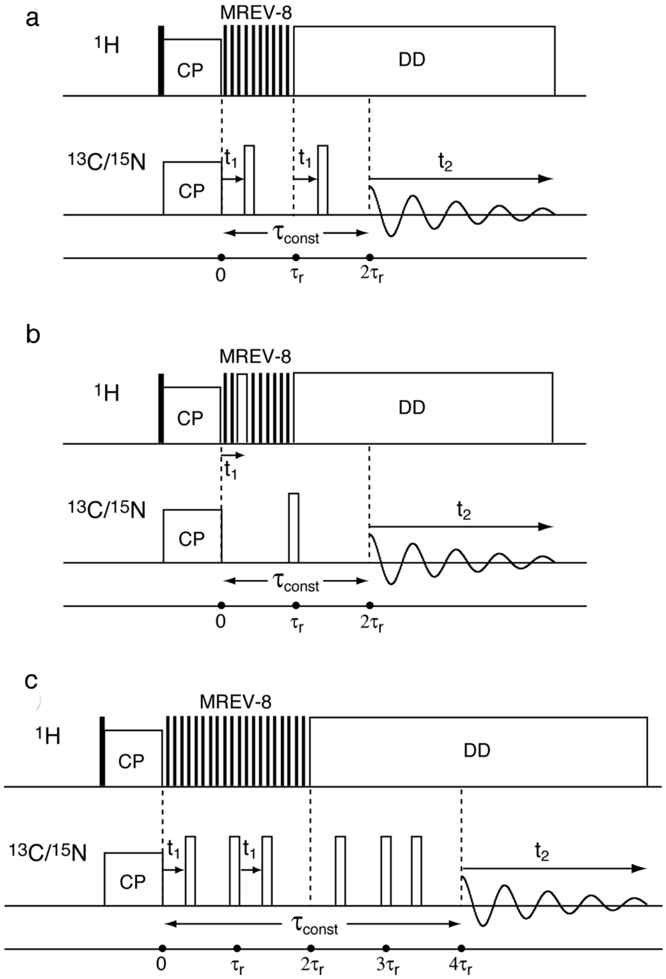

FIG. 1. (a–b) Pulse sequences for doubling the effective X–^{1}H dipolar couplings under MAS. MREV-8 homonuclear decoupling is applied for an entire rotor period in both sequences. (a) Two X 180° pulses are applied at t_1 and $t_1 + \tau_r$. (b) One ^{1}H 180° pulse at t_1 and one X 180° pulse at τ_r are used. (c) Pulse sequence for quadrupling the X–^{1}H dipolar interaction. The MREV-8 multiple-pulse train is applied for two rotor cycles. An X 180° pulse is applied at time t_1 from the beginning of each rotor cycle. A 180° pulse at the end of the first rotor period ensures the proper addition of the dynamic phase associated with each rotor period. Two more rotor periods with the same X pulses but heteronuclear decoupling follow in order to refocus the X-spin chemical shift. In all the sequences filled narrow rectangles represent 90° pulses while the unfilled broad rectangles indicate 180° pulses.

the 180° pulses and the homonuclear decoupling pulses were not synchronized with the rotor cycle, and the evolution period was usually not part of a constant time. As a result, the experiments produced convolutions of spectral patterns with sideband intensities at both ω_r and $\omega_r/2$ (*21*), which are not rigorously identical to the spectra taken at $\omega_r/2$. In addition, the dipolar sidebands were usually mixed with the chemical shift sidebands due to the lack of synchronization and had to be separated by skew projections. However, the separation is not possible in certain cases. The current experiment avoids these complications by limiting the dipolar evolution to an integer multiple of the rotor cycle, thus producing simple dipolar sideband spectra with the envelope identical to that of a sample spinning at $\omega_r/2$.

2. 2n-fold Amplification of the Dipolar Evolution

The basic scheme of doubling the dynamic phase of an NMR interaction can be repeated n times to produce a $2n$-fold increase in the phase, thus amplifying the interaction strength δ_λ by the same factor. For example, to ''quadruple'' the X–^{1}H dipolar coupling, we can employ *two* rotor cycles of proton homonuclear decoupling and an X-spin 180° pulse at time t_1 from the beginning of each rotor cycle (Fig. 1c). Another X-spin 180° pulse must be applied at the end of the first rotor cycle to ensure the addition of the phases associated with each rotor period. To refocus the X chemical shift anisotropy that is also amplified by this point, two more rotor cycles with heteronuclear dipolar decoupling and the same X pulses must be added. The resulting spectrum has sidebands spaced at the actual spinning speed but an intensity envelope identical to that taken at a quarter of the spinning speed. The extendability of this pulse sequence distinguishes it from methods that enhance the sidebands by dipolar decoupling for a fraction of the rotor cycle (*14, 22*).

Higher-order amplification of δ_{XH} is useful in applications where high spinning speeds are desirable, and is limited only by the attainable spectral bandwidth in the ω_1 dimension given the finite pulse lengths on both the ^{1}H and the X channel. For example, using semi-windowless MREV-8 (*23*), a t_1 increment equal to a quarter of the MREV-8 cycle, and high ^{1}H RF powers, it is possible to achieve a dwell time small enough to contain the quadrupled one-bond C–H dipolar coupling. Other homonuclear decoupling sequences with short cycle times such as the frequency-switched Lee–Goldberg sequence may also be employed (*24, 25*). The upper limit of the spinning speeds is about 10 kHz, above which interference effects between multiple-pulse decoupling and sample rotation become significant.

For simplicity, in the remainder of the paper we refer to the X–^{1}H coupling ''doubled'' and ''quadrupled'' DIPSHIFT experiments as $2\Phi_{XH}$- and $4\Phi_{XH}$-DIPSHIFT, respectively.

3. Selective Dipolar ''Doubling'' for Measuring the Torsion Angle ϕ

The coupling amplification method can be incorporated into the recently developed NH/C$^\alpha$H experiment that determines the peptide torsion angle $\phi°$ (*8*). The new pulse sequence, shown in Fig. 2, adopts the approach of separate but synchronous evolutions (*26*). First, antiphase ^{13}C magnetization $C_{x,y}N_z$ is generated after recoupling the N–C dipolar interaction with a short period of REDOR sequence (*27*). $C_{x,y}N_z$ is then allowed to evolve under the C–H dipolar interaction for a duration defined by the length of the MREV-

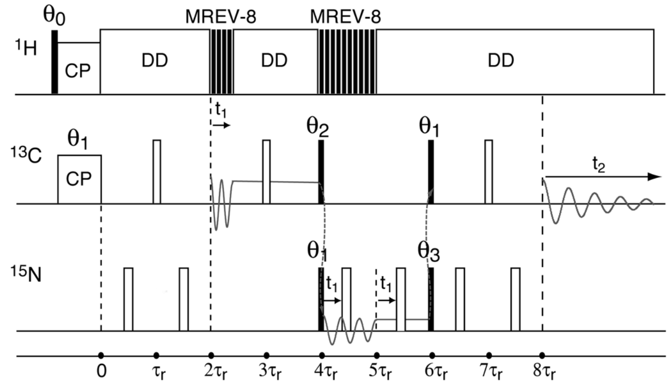

FIG. 2. Pulse sequence for determining the peptide backbone torsion angle ϕ using effectively doubled N–H dipolar coupling. The C–H and N–H dipolar interactions evolve in two separate periods synchronously in order to double the N–H dipolar phase selectively. The C–H coupling is measured by incrementing the MREV-8 multiple-pulse train, while the N–H interaction is measured by moving the ^{15}N 180° pulse through a rotor period with constant MREV-8 decoupling. Antiphase magnetization of the forms C_xN_z and N_xC_z are created by refocusing the ^{13}C– ^{15}N dipolar interaction and simultaneous 90° pulses. The filled rectangles indicate 90° pulses while the unfilled ones represent 180° pulses. The phase cycles are θ_0 = 13, θ_1 = 11223344, θ_2 = 13243142, θ_3 = 13243142 31421324, and receiver = 31421324 13243142, where 1, 2, 3, and 4 represent the four phases x, y, $-x$, and $-y$, respectively.

8 train that decouples the proton homonuclear interaction. Next, two simultaneous 90° pulses on ^{13}C and ^{15}N are applied to transform the density operator to antiphase ^{15}N magnetization, $C_zN_{x,y}$, which evolves under the effectively doubled N–H coupling in the same fashion as in Fig. 1a. The ^{15}N 180° pulses are moved synchronously with the increment of the MREV-8 train during the preceding C–H evolution period, so that the resulting ω_1 dimension of the 2D spectrum reflects both the N–H and the C–H couplings. Finally, the ^{15}N antiphase magnetization is converted to observable ^{13}C magnetization by a combination of 90° pulses and a second REDOR period. The ^{13}C isotropic chemical shift is detected during the t_2 period.

RESULTS AND DISCUSSION

The result of doubling the apparent N–H dipolar couplings in NAV is shown in Fig. 3. The $2\Phi_{NH}$-DIPSHIFT spectrum was obtained with the pulse sequence of Fig. 1a and the normal DIPSHIFT spectrum reflecting the unchanged N–H couplings was taken without the moving 180° pulses (*8*). A spinning speed of 2137 Hz was used in both experiments. The left column shows the t_1 modulations of the ^{15}N resonance, which are the sum of the ω_1 cross sections at the various ^{15}N chemical shift sidebands. As expected, the decay of the time signal of the $2\Phi_{NH}$ experiment (Fig. 3a) is more rapid and greater than that of the normal DIPSHIFT experiment (Fig. 3d). The single-rotor-period time signals are replicated and Fourier transformed to yield rotational sideband spectra, shown in the middle column. The $2\Phi_{NH}$-DIPSHIFT spectrum (Fig. 3b) exhibits significant intensities up to the fourth-order sidebands, and the sideband envelope has two characteristic singularities reminiscent of the Pake pattern that would be obtained without rotation. In comparison, the sideband pattern of the normal DIPSHIFT spectrum (Fig. 3e) shows a more featureless envelope dominated by the centerband. Simulations of the two spectra yield an effective dipolar coupling of 10.2 ± 1.0 kHz for the former (Fig. 3c) and 5.2 ± 0.5 kHz for the latter (Fig. 3f). These effective couplings are the products of the static one-bond (∼1.06 Å) N–H dipolar coupling constant and the scaling factor (∼0.536) of the semi-windowless MREV-8 sequence (*23*). Note that the additional sidebands extending to the two edges of the experimental spectra are noise peaks. They are restricted to multiples of $2\pi/\tau_r$ by the periodic replication of the noise in the time signal.

Figure 4 compares the $4\Phi_{NH}$- and $2\Phi_{NH}$-DIPSHIFT spectra of NAV. They were taken at $\omega_r/2\pi$ = 2778 Hz with a t_1 dwell time of 9 μs. This short dwell time is necessary for accommodating the increased dipolar coupling in the ω_1 dimension, and was achieved by incrementing a quarter of the semi-windowless MREV-8 cycle per t_1 point, using a ^{1}H 90° pulse of 3 μs. The best-fit simulations yield effective N–H couplings of 24.0 ± 2.0 and 11.3 ± 1.0 kHz for the $4\Phi_{NH}$ and $2\Phi_{NH}$ spectra, respectively. Small deviations in the center of the spectrum are observed between the experimental and the simulated $4\Phi_{NH}$-DIPSHIFT spectra (Figs. 4a and 4b). They may arise from long-range N–H couplings which are not adequately included in the simulations.

We incorporated the coupling amplification method into the measurement of the peptide torsion angle ϕ. Figure 5

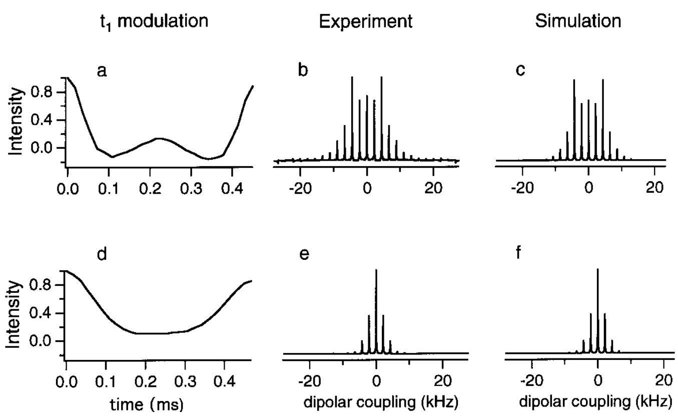

FIG. 3. Interaction ''doubling.'' (a–c) $2\Phi_{NH}$-DIPSHIFT spectrum and (d–f) normal DIPSHIFT spectrum of NAV. A spinning speed of 2137 Hz was used. Both the t_1 signals and the ω_1 spectra are sums of the cross sections at the ^{15}N chemical shift sidebands. The decay of the time signal in the $2\Phi_{NH}$ experiment (a) is more rapid and greater than that in the coupling unchanged experiment (d). Correspondingly, the $2\Phi_{NH}$-DIPSHIFT spectrum (b) displays more rotational sidebands than the normal spectrum (e). Simulations indicate that the effective couplings are 10.2 ± 1.0 kHz (c) and 5.2 ± 0.5 kHz (f), respectively.

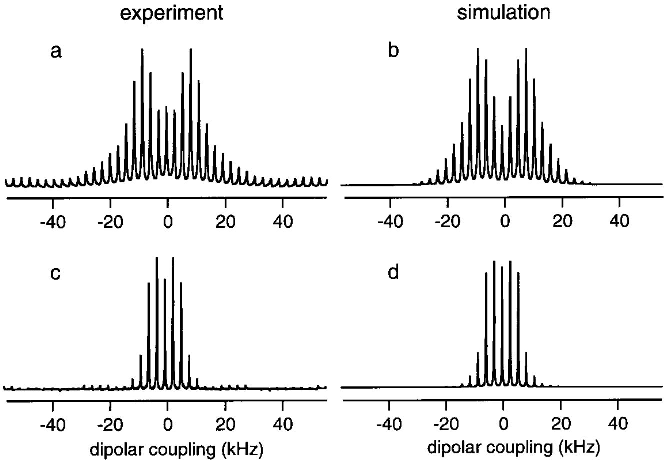

FIG. 4. Interaction ''quadrupling.'' (a) $4\Phi_{NH}$-DIPSHIFT spectrum of NAV taken at $\omega_r/2\pi = 2778$ Hz. (b) The best-fit simulation indicates $\omega_{NH} = 24.5 \pm 2.0$ kHz, which is the product of $4\delta_{NH}$ and the MREV-8 scaling factor. (c–d) The corresponding $2\Phi_{NH}$-DIPSHIFT spectrum and simulation with 11.3 ± 1.0 kHz.

displays the $2\Phi_{NH}$-NH/C$^\alpha$H spectrum of NAV. The ω_2 dimension (Fig. 5a) exhibits only the C$^\alpha$ and acetyl carbonyl resonances due to the short N–C dipolar recoupling period used. The t_1 oscillation of the C$^\alpha$ resonance (Fig. 5b) was replicated and Fourier transformed to give a sideband spectrum (Fig. 5c) that is indicative of the relative orientation of the N–H^N and C$^\alpha$–H$^\alpha$ bonds. Due to the effective doubling of the N–H dipolar coupling, the spectrum shows greater intensities at the first- and second-order sidebands compared to the original experiment (*8*). The best-fit simulation (Fig. 5d) was achieved with a torsion angle $\phi = -142° \pm 5°$, in fair agreement with the X-ray result of $\phi = -136.5°$ (*28*).

To demonstrate the sensitivity of the $2\Phi_{NH}$-NH/C$^\alpha$H experiment to the torsion angle ϕ, we display a series of calculated spectra for ϕ ranging from 60° to −120° in 20° increments (Fig. 6). The spectral patterns vary more significantly than those without the doubled N–H coupling (*8*), which indicates improved angular resolution. The largest ϕ dependence is observed in the β-sheet region. As described previously, due to the uniaxiality of the dipolar interaction, each spectrum corresponds to two torsion angles ϕ_1 and ϕ_2 that are related by $(\phi_1 + \phi_2)/2 = -120°$ (*8*).

To obtain a more quantitative estimate of the angular resolution, we calculated the root-mean-squared deviations (RMSDs) for each pair of spectra and represented them as 2D contour plots, where both axes indicate the torsion angle ϕ (Fig. 7). The RMSD between spectra $S(\phi_1)$ and $S(\phi_2)$ is defined as

$$\mathrm{RMSD}(\phi_1, \phi_2) = \left\{\frac{1}{N}\sum_{i=1}^{N}[S_i(\phi_1) - S_i(\phi_2)]^2\right\}^{1/2}, \quad [5]$$

where $S_i(\phi)$ represents the spectral intensity of the ith sideband, and N is the number of independent sidebands in the spectrum. The RMSDs of both the original NH/C$^\alpha$H experiment and the $2\Phi_{NH}$-NH/C$^\alpha$H experiment are calculated and compared. The contour levels used in the two plots range from 0 to 100% of the largest value, which occurs in the $2\Phi_{NH}$-NH/C$^\alpha$H experiment, at 5% intervals. The contour level of the diagonal is zero, since $S_i(\phi) - S_i(\phi) = 0$. Away from the diagonal, the contour heights are finite, indicating nonvanishing differences between the spectra. The higher the contour intensity, the larger the spectral difference. The larger the slope, the higher the angular resolution. For both experiments, the highest angular resolution is observed around $\phi = -120°$, corresponding to the extended β-sheet structure, and the lowest resolution occurs near $\phi = 60°$, corresponding to the rarely occurring left-handed α-helix. Although these qualitative features of the two contour plots are similar, it is important to note that the contour heights for the N–H coupling doubled experiment (Fig. 7b) are more than a factor of 2 greater than those of the original experiment (Fig. 7a). This indicates an enhancement of the ϕ resolution throughout the entire angular range due to the selective amplification of the N–H coupling. Some cross sections of each contour plot are also displayed in Fig. 7 to enable better visualization of the 2D plots.

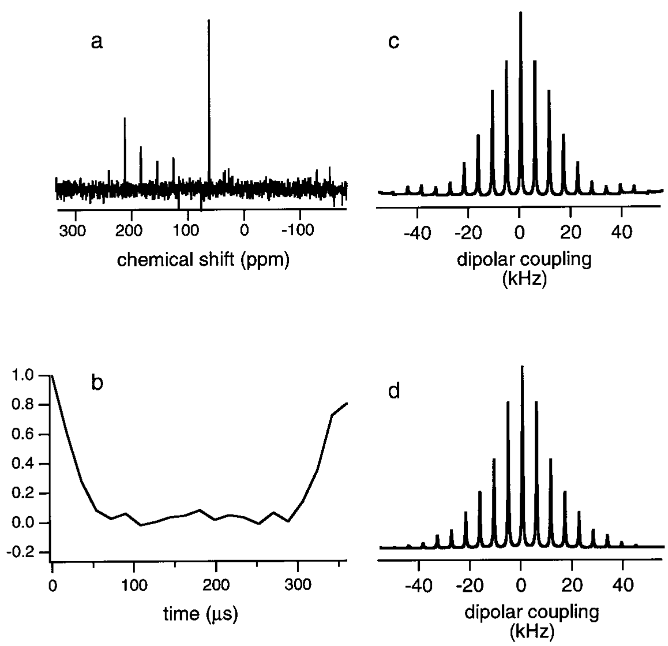

FIG. 5. $2\Phi_{NH}$-NH/C$^\alpha$H spectrum of NAV taken at $\omega_r/2\pi = 2778$ Hz for determining the torsion angle ϕ. From the C$^\alpha$ resonance in the ω_2 spectrum (a), we extracted the t_1 oscillation for one rotor period (b), replicated it, and Fourier transformed it to produce a dipolar sideband spectrum (c) that is indicative of the relative orientation of the N–H^N and the C$^\alpha$–H$^\alpha$ bonds. Simulation (d) yields $\phi = -142° \pm 5°$. The data were acquired with 512 scans for each of the 17 t_1 points. The signal averaging time was 8 h.

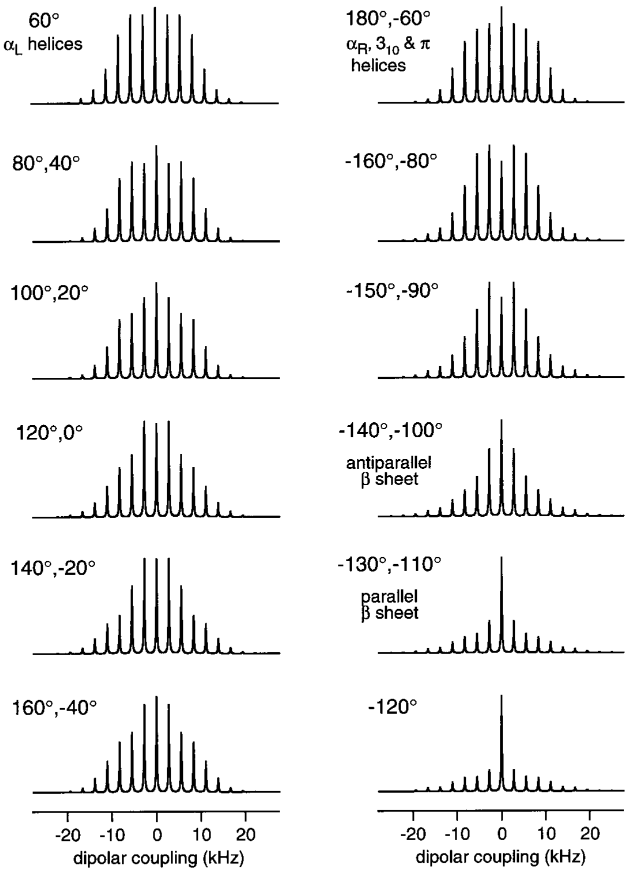

FIG. 6. Simulated $2\Phi_{NH}$-NH/C$^{\alpha}$H spectra as a function of the torsion angle ϕ at $\omega_r/2\pi = 2778$ Hz. Compared with the spectra without the doubled N–H coupling (*8*), the spectral variation with ϕ is more drastic, indicating higher angular resolution. Each spectrum corresponds to two ϕ angles due to the uniaxial symmetry of the dipolar interaction. Input parameters for the simulation are $\omega_{CH} = 10.8$ kHz, $\omega_{NH} = -11.3$ kHz, $\omega_r/2\pi = 2778$ Hz, 5000 crystallite orientations, and various Euler angles $\beta_{PM}^{CH} = 109.5°$, $\beta_{PM}^{NH} = 60°$, $\gamma_{PM}^{CH} = 0°$, and $\gamma_{PM}^{NH} = \phi_H = \phi - 60$, where the subscript PM indicates rotation from the principle axis frame of the dipolar tensor to the molecular frame. The molecular frame is defined with its *z*-axis collinear with the N–C$^{\alpha}$ bond (*8*), and the β and γ angles are defined according to Spiess' convention (*29*).

The RMSD calculation can be similarly employed to obtain a more quantitative estimate of the error margin of the experimentally determined ϕ value. Namely, we can calculate the RMSDs between the experimental and the various simulated spectra and plot them in a 1D curve where the *x*-axis represents ϕ. The minimum of the curve thus corresponds to the best-fit torsion angle, while the breadth of the ''valley'' defined by the intersection of the experimental RMS noise and the curve indicates the random error of the measurement. The experimental RMS noise can in turn be estimated from the noise sidebands observed at the two edges of the spectra, where no signals are expected from the simulations. In this way, we found the normal NH/C$^{\alpha}$H experiment to have an uncertainty of ±7° around −135° or −105°, while the $2\Phi_{NH}$-NH/C$^{\alpha}$H experiment gave an uncertainty of ±5° around −142° or −98°. Like other methods of statistical error analysis, the systematic error of the measurement is not taken into account.

CONCLUSIONS

We demonstrated the amplification of the apparent magnitudes of X–^{1}H dipolar interactions in MAS experiments. This was achieved by moving 180° pulses during one or more rotor periods of constant proton homonuclear decoupling. The technique allows dipolar couplings to be determined at relatively high spinning speeds, which are necessary for resolving chemically inequivalent sites in high magnetic fields. Examples of ''doubling'' and ''quadrupling'' dipolar couplings are shown for the one-bond N–H coupling in *N*-acetyl-D,L-valine. We also showed a useful application of the technique to the measurement of the peptide backbone torsion angle ϕ through NH/C$^{\alpha}$H dipolar correlation. Using separate and synchronous evolutions of the C–H and N–H dipolar interactions, we selectively amplified the N–H coupling, thus increasing the ϕ dependence of the dipolar spectra significantly. An RMSD analysis is employed to quantitate the resolution enhancement of the N–H coupling-doubled NH/C$^{\alpha}$H experiment compared to the original version.

EXPERIMENTAL

All experiments were performed on a 9.4-T custom-designed spectrometer equipped with a triple-resonance transmission-line probe (*31–33*) with a 4-mm Chemagnetics (Fort Collins, CO) MAS spinning module. The transmission-line design enables high RF powers to be attained on all three channels without arcing. Proton RF fields of about 100 kHz were used for excitation and CW decoupling. CP spin lock was achieved at lower RF fields of about 40 to 55 kHz. The ^{1}H 90° pulse length for MREV-8 multiple-pulse decoupling was about 3.0 μs. The semi-windowless version of MREV-8 was used and incremented either in half or in quarter cycles, depending on the required spectral width of the ω_1 dimension. ^{13}C and ^{15}N 90° pulse lengths were typically 4 and 6 μs, respectively. The spinning speeds were controlled to ±5 Hz by a Doty (Columbia, SC) spinning speed controller. The recycle delay was 2.5 s. A cross-polarization time of 2 ms was used.

Powder ^{15}N-labeled *N*-acetyl-D,L-valine was purchased from Cambridge Isotope Laboratories (Andover, MA) and recrystallized from aqueous solution to reduce chemical shift dispersions due to conformational heterogeneity. Approximately 40 mg of sample was used in the experiments.

Simulations of the various dipolar spectra were performed in the time domain by evaluating the MAS dynamic phases over the course of the evolution period t_1. Powder averaging was carried out by Monte Carlo integration where the Euler angles that transform the molecular frame to the rotor frame are randomly generated according to a powder distribution.

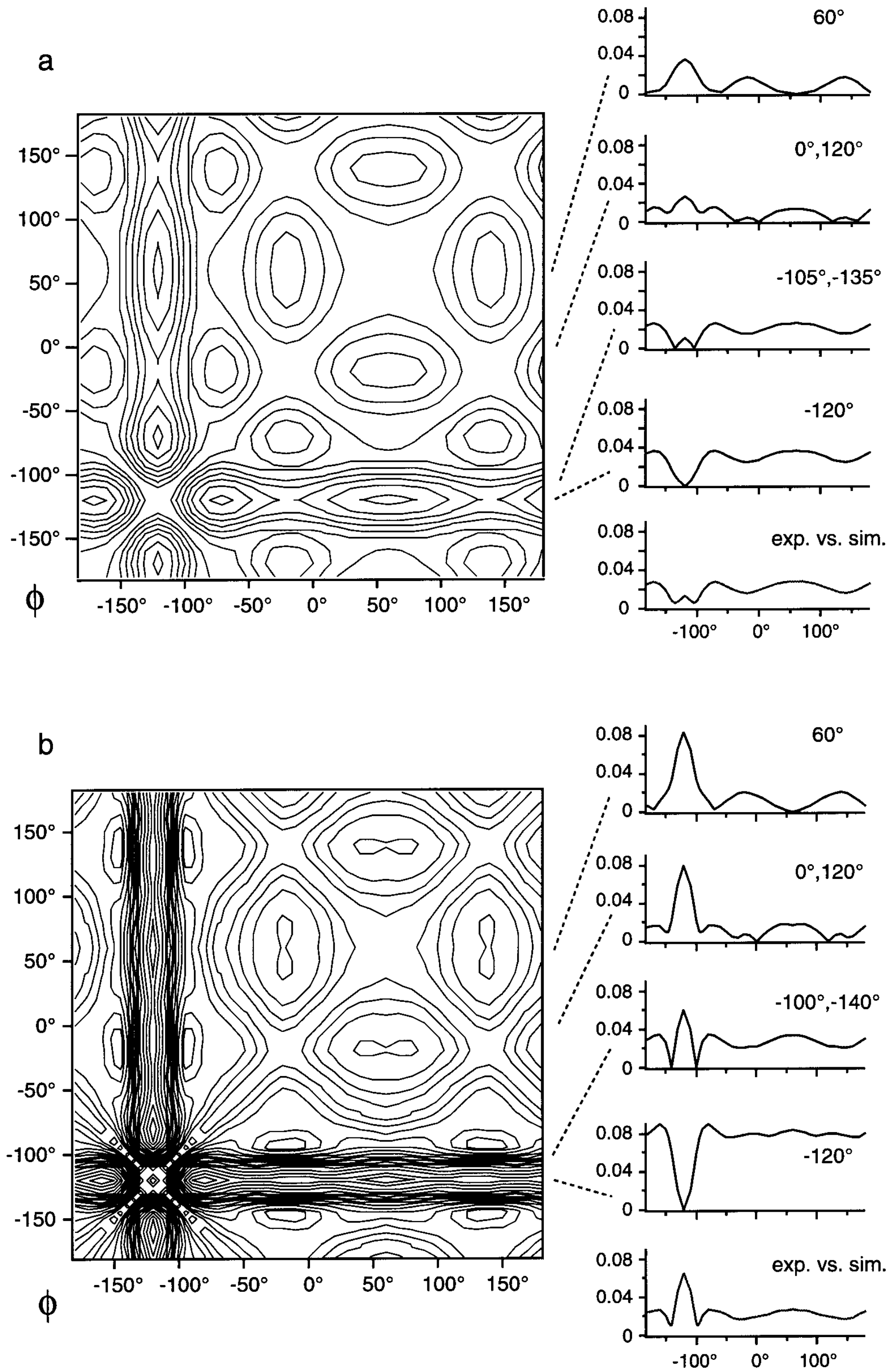

FIG. 7. Angular resolution of the NH/C$^{\alpha}$H experiments for the determination of ϕ. Contour levels represent the RMSDs between a pair of simulated spectra $S(\phi_1)$ and $S(\phi_2)$. Contour heights range from 0 to 100% of the highest RMSD value at 5% intervals. (a) Normal NH/C$^{\alpha}$H experiment. (b) $2\Phi_{NH}$-NH/C$^{\alpha}$H experiment. Vanishing RMSDs are obtained along the diagonal of each plot, as required for identical spectra. The largest RMSDs occur around $\phi = -120°$ in both experiments. The RMSDs of the $2\Phi_{NH}$ experiment are more than twice those of the original experiment, indicating higher ϕ resolution. Some cross sections of each plot are shown, along with the RMSD curve between the experiment and the simulations. The experimental result without doubled N–H coupling is taken from Ref. (*8*).

Input parameters for the torsion angle simulations include the effective C–H and N–H dipolar couplings, which were obtained from control ^{15}N and ^{13}C DIPSHIFT experiments (*8*), various Euler angles, the REDOR mixing time, the spinning speed ω_r, the spectral width, and the number of crystallites employed in the powder average. The centerband and 12 sidebands (6 on either side) were included in the RMSD fits (*30*).

ACKNOWLEDGMENTS

The experiments conducted at MIT were supported by the National Institute of Health (GM-23403, GM-23289, and RR-00995). M. Hong was supported by a NIH postdoctoral fellowship (GM-18870). K.Schmidt-Rohr gratefully acknowledges generous support from the Arnold and Mabel Beckman Foundation. C. M. Rienstra is a Howard Hughes Medical Institute Predoctoral Fellow.

REFERENCES

1. J. E. Roberts, G. S. Harbison, M. G. Munowitz, J. Herzfeld, and R. G. Griffin, Measurement of heteronuclear bond distances in polycrystalline solids by solid-state NMR techniques, *J. Am. Chem. Soc.* **109,** 4163–4169 (1987).
2. M. Linder, A. Hoehener, and R. R. Ernst, Orientation of tensorial interactions determined from two dimensional NMR powder spectra, *J. Chem. Phys.* **73,** 4959–4970 (1980).
3. M. G. Munowitz, R. G. Griffin, G. Bodenhausen, and T. H. Huang, Two-dimensional rotational spin-echo NMR in solids: Correlation of chemical shift and dipolar interactions, *J. Am. Chem. Soc.* **103,** 2529–2533 (1981).
4. M. Hong, K. Schmidt-Rohr, and A. Pines, Measurement of signs and magnitudes of C–H dipolar couplings in lecithin, *J. Am. Chem. Soc.* **117,** 3310–3311 (1995).
5. J. D. Gross, D. E. Waschawski, and R. G. Griffin, Dipolar recoupling in MAS NMR: A probe for segmental order in lipid bilayers, *J. Am. Chem. Soc.* **119,** 796–802 (1997).
6. B. M. Fung, J. Afzal, T. L. Foss, and M. Chau, Nematic ordering of 4-*n*-alkyl-4′-cyanobiphenyls studied by carbon-13 NMR with off-magic-angle spinning, *J. Chem. Phys.* **85,** 4808–4814 (1986).
7. X. Feng, Y. K. Lee, D. Sandstroem, M. Eden, H. Maisel, A. Sebald, and M. H. Levitt, Direct determination of a molecular torsional angle by solid-state NMR, *Chem. Phys. Lett.* **257,** 314–320 (1996).
8. M. Hong, J. D. Gross, and R. G. Griffin, Site-resolved determination of peptide torsion angle phi from the relative orientations of backbone N–H and C–H bonds by solid-state NMR, *J. Phys. Chem. B* **101,** 5869–5874 (1997).
9. X. Feng, P. J. E. Verdegem, Y. K. Lee, D. Sandstrom, M. Eden, P. Bovee-Geurts, W. J. d. Grip, J. Lugtenburg, H. J. M. d. Groot, and M. H. Levitt, Direct determination of a molecular torsion angle in the membrane protein Rhodopsin by solid-state NMR, *J. Am. Chem. Soc.* **119,** 6853–6857 (1997).
10. W. T. Dixon, Spinning-sideband-free and spinning-sideband-only NMR spectra in spinning samples, *J. Chem. Phys.* **77,** 1800–1809 (1982).
11. J. Hong and G. S. Harbison, Magic angle spinning sideband elimination by temporary interruption of the chemical shift, *J. Magn. Reson.* **105,** 128–136 (1993).
12. Z. Song, O. N. Antzutkin, X. Feng, and M. H. Levitt, Sideband suppression in magic-angle spinning NMR by a sequence of 5 pi pulses, *Solid State NMR* **2,** 143–146 (1993).
13. T. Gullion and J. Schaefer, Detection of weak heteronuclear dipolar coupling by rotational-echo double-resonance nuclear magnetic resonance, *in* ''Advances in Magnetic Resonance'' (W. S. Warren, Ed.), pp. 57–83, Academic Press, San Diego (1989).
14. V. Bork, T. Gullion, A. Hing, and J. Schaefer, Measurement of ^{13}C–^{15}N couplings by dipolar-rotational-spin-echo NMR, *J. Magn. Reson.* **88,** 523–532 (1990).
15. M. G. Munowitz and R. G. Griffin, Two-dimensional NMR in rotating solids: Time reversal effects in chemical shift-dipolar spectra, *J. Chem. Phys.* **78,** 613–617 (1983).
16. D. P. Raleigh, A. C. Kolbert, T. G. Oas, M. H. Levitt, and R. G. Griffin, Enhancement of the effect of small anisotropies in magic-angle spinning NMR, *J. Chem. Soc. Faraday Trans. 1* **84,** 3691–3711 (1988).
17. E. T. Olejniczak, S. Vega, and R. G. Griffin, Multiple pulse NMR in rotating solids, *J. Chem. Phys.* **81,** 4804–4817 (1984).
18. M. M. Maricq and J. S. Waugh, NMR in rotating solids, *J. Chem. Phys.* **70,** 3300–3316 (1979).
19. A. C. Kolbert, D. P. Raleigh, M. H. Levitt, and R. G. Griffin, Two-dimensional spin-echo nuclear magnetic resonance in rotating solids, *J. Chem. Phys.* **90,** 679–689 (1989).
20. A. C. Kolbert, H. J. M. d. Groot, M. H. Levitt, M. G. Munowitz, J. E. Roberts, G. S. Harbison, J. Herzfeld, and R. G. Griffin, Two-dimensional dipolar-chemical shift NMR in rotating solids, *in* ''Multinuclear Magnetic Resonance in Liquids and Solids–Chemical Applications'' (P. Granger and R. K. Harris, Eds.), pp. 339–354, Kluwer Academic, Dordrecht, The Netherlands (1990).
21. A. C. Kolbert and R. G. Griffin, Two-dimensional spin-echo dipolar-sideband enhancement in magic-angle-spinning NMR, *J. Magn. Reson.* **93,** 242–255 (1991).
22. M. E. Merritt, A. M. Christensen, K. J. Kramer, T. L. Hopkins, and J. Schaefer, Detection of intercatechol cross-links in insect cuticle by solid-state carbon-13 and nitrogen-15 NMR, *J. Am. Chem. Soc.* **118,** 11278–11282 (1996).
23. W.-K. Rhim, D. D. Elleman, and R. W. Vaughan, MREV-8, *J. Chem. Phys.* **59,** 1740 (1973).
24. A. Bielecki, A. C. Kolbert, and M. H. Levitt, Frequency-switched pulse sequences: Homonuclear decoupling and dilute spin NMR in solids, *Chem. Phys. Lett.* **155,** 341–346 (1989).
25. M. Lee and W. I. Goldberg, Nuclear-magnetic-resonance line narrowing by a rotating rf field, *Phys. Rev. A* **140,** 1261–1271 (1965).
26. M. Hong, A. Pines, and S. Caldarelli, Measurement and assignment of long-range C–H dipolar couplings in liquid crystals by two-dimensional NMR spectroscopy, *J. Phys. Chem.* **100,** 14815–14822 (1996).
27. T. Gullion and J. Schaefer, Rotational echo double resonance NMR, *J. Magn. Reson.* **81,** 196–200 (1989).
28. P. J. Carroll, P. L. Stewart, and S. J. Opella, Structures of two model peptides: *N*-acetyl-D,L-valine and *N*-acetyl-L-valyl-L-leucine, *Acta Crystallogr. C* **46,** 243–246 (1990).
29. H. W. Spiess, Rotation matrices, *in* ''NMR Basic Principles and Progress'' (P. Diehl, E. Fluck, and E. Kosfeld, Eds.), Springer, Berlin (1978).
30. Including sidebands further out, where all the simulated spectra show negligible intensity, would change neither the position nor the shape of the minimum in the rmsd curve. Thus the best-fit angle and its error margin would remain unchanged. It would only add an offset to the whole rmsd curve, due to the constant deviation between the experimental noise and the nearly vanishing intensity in the simulated spectra at these outer sidebands.
31. R. A. McKay, U.S. Patent 4,446,431.
32. S. M. Holl, R. A. McKay, T. Gullion, and J. Schaefer, Rotational-echo triple-resonance NMR, *J. Magn. Reson.* **89,** 620–626 (1990).
33. R. A. McKay, private communication.